

# Optimization of Numerical Algorithms for Solving Inverse Problems of Ultrasonic Tomography on a Supercomputer

Sergey Romanov

Lomonosov Moscow State University, Moscow, Russia  
romanov60@gmail.com

**Abstract.** The paper is dedicated to optimizing numerical algorithms to solve wave tomography problems by using supercomputers. The problem is formulated as a non-linear coefficient inverse problem for the wave equation. Due to the huge amount of computations required, solving such problems is impossible without the use of high-performance supercomputers. Gradient iterative methods are employed to solve the problem. The gradient of the residual functional is calculated from the solutions of the direct and the "conjugate" wave-propagation problems with transparent boundary conditions. Two formulations of the transparency condition are compared. We show that fourth-order finite-difference schemes allow us to reduce the size of the grid by a factor of 1.5–2 in each coordinate compared to second-order schemes. This makes it possible to significantly reduce the amount of computations and memory required, which is especially important for 3D problems of wave tomography. The primary application of the method is medical ultrasonic tomography.

**Keywords:** Ultrasound · Coefficient inverse problems · Supercomputer · Wave tomography · Finite-difference schemes

## 1 Introduction

Currently, intensive works are being carried out to develop new tomographic devices that use wave radiation sources. The most promising technology is ultrasonic tomography. The most important applications of ultrasonic tomography are in medical research, primarily the differential diagnosis of breast cancer, which is one of the most pressing issues of medical diagnostics. Wave tomography technology can also be used in many other applications, such as seismic studies, non-destructive testing, and medical ultrasonic imaging [1-3].

One of the problems in the development of ultrasonic tomography is associated with the nonlinearity of inverse problems of wave tomography. These inverse problems are formulated as coefficient inverse problems for the wave equation [4,5]. The developments of ultrasonic tomography devices are currently at the stages of modeling and prototypes [6-8]. These works employ simplified mathematical models. The most promising approach is to develop methods for solving inverse problems of wave

tomography under models that account for both wave diffraction effects (diffraction, refraction, multiple scattering) and absorption. The derivation of the gradient of the residual functional of the coefficient inverse problem, as obtained in [9-14], was the breakthrough result in this field.

The approximate gradient-based methods for solving inverse problems of ultrasonic tomography have been developed in [15-19]. The developed algorithms are designed for supercomputers. These algorithms implement iterative gradient methods to minimize the residual functional between the wave field measured experimentally and the numerically simulated wave field. To calculate the gradient of the residual functional at each iteration of the method, it is necessary to solve the "direct" problem of simulating the wave propagation process in an inhomogeneous medium in forward time and the "conjugate" problem in reverse time. The efficiencies of the developed numerical methods were evaluated by benchmarking numerous model problems on the "Lomonosov" supercomputer. The developed methods allow effective parallelization. The numerical algorithms practically linearly scale with the number of processors in CPU- and GPU-based systems.

The aim of this study is to optimize the developed numerical algorithms. The first way to optimize the algorithms is to use a finite-difference scheme. The numerical methods for solving the inverse problem of wave tomography that have been implemented in the previous works are based on the finite-difference time-domain (FDTD) method that provides a second-order approximation of the wave equation. The FDTD method has been chosen because it has a very large potential for relatively simple parallelization of computations. Because of the large amount of computations, highly parallel computing is required. Supercomputer technologies drastically reduce the computation time required to solve inverse problems. However, one of the issues is the accuracy of the calculations. To solve the ill-posed inverse problems of wave tomography, very high accuracy is required. For second-order FDTD schemes, this leads to the need to use very large grids. With the increase of the sounding frequencies, the volume of data becomes unacceptably large. This is especially true for 3D problems, where high-performance GPU processors are required, and GPUs have a limited memory capacity. Additionally, there are numerical error accumulation issues associated with large grids.

For second-order FDTD schemes, it is necessary to use at least  $n=1000$  grid points in each coordinate for the numerical error to be no more than a few percent. In the 3D version of the method, this results in a  $1000^3$ -point grid. Even when solving such problems on powerful GPU clusters, such an amount of data does not fit into the internal memory of the GPU devices. Another problem is the dependence of the number of operations in the gradient iterative algorithms on the number of grid points, which is of the form  $O(n^4)$ . A fourth power of  $n$  means that whereas it takes one hour to solve a 3D problem for  $n=400$  on a GPU cluster, it would take approximately 5 hours to solve a problem for  $n=600$ . Therefore, one of the ways to optimize the algorithms is to use higher-order approximations. As will be shown, using a fourth-order approximation scheme results in a decrease in the number of grid points  $n$  by a factor of 1.5–2, which significantly reduces the computation time.

The second important issue is the problem of boundary conditions. This problem arises because we have to solve direct and inverse problems in a bounded domain. As a result, reflection of waves occurs at the boundary of the computational domain. In this paper, two methods of implementing a “transparent” boundary are considered.

The third issue is that the inverse problem of wave tomography typically has incomplete input data — the sources and detectors are not located on all sides of the studied object. In ultrasonic mammography applications, the data incompleteness results from the fact that we cannot place sources and detectors at the patient’s chest-wall side. Thus, it is an incomplete-data tomography.

## 2 Formulation of the Inverse Problem of Ultrasonic Tomography with Incomplete Data and Solution Methods

Let us consider the "direct" problem of computing the acoustic pressure  $u(\mathbf{r}, t)$  for the time  $(0; T)$  in the region  $\Omega \subset \mathbb{R}^N$  ( $N = 2, 3$ ), bounded by the surface  $\partial\Omega$  (Fig. 1), with a point source at the point  $\mathbf{r}_0$ :

$$c(\mathbf{r})u_{tt}(\mathbf{r}, t) - \Delta u(\mathbf{r}, t) = \delta(\mathbf{r} - \mathbf{r}_0) g(t). \quad (1)$$

Let us assume that  $u(\mathbf{r}, t)$  satisfies the zero initial and boundary conditions

$$u(\mathbf{r}, t = 0) = u_t(\mathbf{r}, t = 0) = 0, \quad \partial_n u(\mathbf{r}, t) / \partial\Omega = 0. \quad (2)$$

Here,  $c^{-0.5}(\mathbf{r}) = v(\mathbf{r})$  is the sound speed in the medium,  $\mathbf{r} \in \mathbb{R}^N$ ;  $\Delta$  is the Laplace operator with respect to  $\mathbf{r}$ . The pulse generated by the source is described by the function  $g(t)$ ;  $\partial_n u(\mathbf{r}, t) / \partial\Omega$  is the derivative along the normal to the boundary  $\partial\Omega$ . It is assumed that the inhomogeneities of the medium are sound-speed variations and are localized within the studied object  $G$ . Outside of the object,  $v(\mathbf{r}) = v_0$  is constant and  $v_0$  is known. The acoustic pressure is measured at the boundary of the domain  $R$ ,  $G \subset R$ . The sources insonify the studied object from different directions. We assume that the sources and the region  $R$  are located far enough from the boundary  $\partial\Omega$  such that the conditions (2) are satisfied.

Fig. 1 illustrates the arrangement of sources and detectors in the two-dimensional inverse problem of wave tomography. The number 1 denotes the positions of the sources of ultrasound waves, and the measurements are taken at the boundary  $\partial R$ . The studied object  $G$  is located inside the domain  $R$ , which is filled with a homogeneous medium with a known sound speed  $v_0$ .

The inverse problem consists of determining the sound speed  $c(\mathbf{r})$  from the experimental data  $U(s, t)$  measured at the boundary  $\partial R$  of the domain  $R$  during the time  $(0, T)$  with different positions  $\mathbf{r}_0$  of the source. In the formulation with incomplete data, the acoustic pressure  $U(s, t)$  is not measured on the whole boundary  $\partial R$ . The

inverse problem with incomplete data can be formulated as a problem of minimizing the residual functional

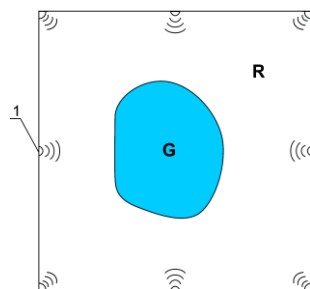


**Fig. 1.** The scheme of the 2D experiment.

$$\Phi(u(c)) = \frac{1}{2} \sum_{j=1}^M \int_0^T \int_{\partial R} E^2(s,t) ds dt, \quad (3)$$

$$\text{where } E(s,t) = \begin{cases} u(\mathbf{s},t) - U(\mathbf{s},t), & \text{for } \mathbf{s} \in \partial R, \text{ where } U(\mathbf{s},t) \text{ is known} \\ 0, & \text{otherwise} \end{cases}. \quad (4)$$

Here,  $u^j(c)$  is the solution of the problem (1)–(2) for some  $c(\mathbf{r})$ ; the index  $j=1, \dots, M$  denotes the position of the source. The inverse problem is formulated as the problem of finding a function  $\bar{c}(\mathbf{r})$  that minimizes the residual functional

$$\min_{c(\mathbf{r})} \Phi(u(c)) = \Phi(u(\bar{c})).$$

Let us consider another problem, which we call "conjugate" to the "direct" problem (1)–(2):

$$c(\mathbf{r})w_n(\mathbf{r},t) - \Delta w(\mathbf{r},t) = E(\mathbf{r},t) \Big|_{r \in \partial R}, \quad (5)$$

$$w(\mathbf{r},t=T) = w_t(\mathbf{r},t=T) = 0, \quad \partial_n w(\mathbf{r},t) \Big|_{\partial \Omega} = 0, \quad (6)$$

where  $E(\mathbf{r},t)$  from (4) is derived from the measured data  $U(s,t)$  and the solution  $u$  of the direct problem (1)–(2). Then, as shown in [9,11,14], the gradient of the functional (3) has the form

$$\Phi'(u(c), dc) = \sum_{j=1}^M \int_{\Omega} \left\{ \left[ \int_0^T w_t^j(\mathbf{r},t) u_t^j(\mathbf{r},t) dt \right] dc(\mathbf{r}) \right\} d\mathbf{r}, \quad (7)$$

where  $u^j$  is the solution of the "direct" problem (1)–(2) and  $w^j$  is the solution of the "conjugate" problem (5)–(6) for the  $j$ -th position of the source.

In contrast to [9,11,14], in the above formulation, the experimental data may be absent on some part of the boundary surrounding the object. Such incomplete data prob-

lems are typical in ultrasonic tomography. For example, in ultrasonic mammography the data cannot be measured at the chest-wall side. Nevertheless, the expression for the gradient (7) is mathematically exact. The formulations of the "direct" and "conjugate" problems considered in this paper also differ from those used in previous works [9,11,14].

### 3 Numerical Algorithms for Solving Inverse Problems of Ultrasonic Tomography

#### 3.1 Finite-Difference Approximations of the Wave Equation

To solve the coefficient inverse problem for the wave equation, we used a finite-difference time-domain method (FDTD). In this formulation, solving the differential wave equation reduces to solving finite-difference equations. Let us present the discretization scheme of the problem in the two-dimensional case. On the computational domain defined by the spatial coordinates  $(x, y)$  and the time  $t$ , we introduce a uniform discrete grid with a space step of  $h$  and a time step of  $\tau$ . To approximate the second-order partial derivatives in equation (1), we use second-order finite differences. We obtain the following explicit finite-difference scheme for equation (1) for the region that does not contain any sources:

$$u_{ij}^{k+1} = \frac{1}{c_{ij}} \tau^2 \Delta u_{ij}^k + 2u_{ij}^k - u_{ij}^{k-1}, \quad (8)$$

where  $\Delta u_{ij}^k = \frac{u_{i+1j}^k - 2u_{ij}^k + u_{i-1j}^k}{h^2} + \frac{u_{ij+1}^k - 2u_{ij}^k + u_{ij-1}^k}{h^2}$  is the discrete Laplacian,  $u_{ij}^k$  are the values of  $u(\mathbf{r}, t)$  at the point  $(i, j)$  at the time step  $k$ , and  $c_{ij}$  are the values of  $c(\mathbf{r})$  at the point  $(i, j)$ . The parameters  $h$  and  $\tau$  are connected by the Courant stability condition  $c^{-0.5} \tau < h / \sqrt{2}$  for a 2D problem. The "conjugate" problem (5)–(6) is computed using a similar FDTD scheme.

This explicit 2<sup>nd</sup>-order FDTD scheme for the wave equation is the simplest and is quite effective for the numerical simulation of wave propagation on a supercomputer. Nevertheless, when the ultrasound pulse propagates distances much larger than the wavelength, the errors of the finite-difference approximation accumulate, which leads to dispersion of the wave. One of the ways to overcome the numerical dispersion is to increase the number of grid points. Model calculations showed that for typical problems of ultrasonic mammography, 25–30 grid points per wavelength are required to obtain sufficient precision. This means that the computational grid size should be approximately  $n=1000$  points in each spatial coordinate and in time. In the 2D case, such grid sizes do not pose a problem for modern supercomputers. However, in the 3D case, the amount of computation grows as  $n^4$  and the required memory capacity grows as  $n^3$ . A large grid size in the 3D case requires a very large number of computing nodes and faces memory size limitations on the GPU processors.

One possible approach to resolving this issue in ultrasonic tomography problems is to increase the accuracy of the finite-difference approximation, which would reduce the size of the grid, the amount of computations and the required memory capacity while maintaining the accuracy of the calculations. In this paper, the use of fourth-order FDTD schemes is considered. Model calculations were performed to compare the performances of second- and fourth-order FDTD schemes for the wave tomography problem.

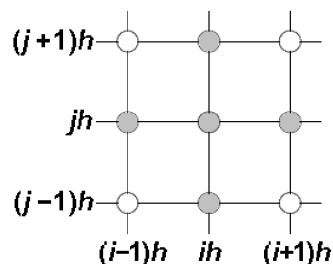


**Fig. 2.** The stencil of the second-order 2D FDTD scheme.

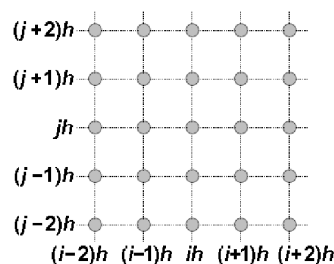


**Fig. 3.** The stencil of the fourth-order 2D FDTD scheme.

Following the work [20], we construct a 2D FDTD scheme that provides fourth-order accuracy with respect to the spatial coordinates. This FDTD scheme is shown in Fig. 3. It has the following general form:

$$\begin{aligned}
 u_{ij}^{k+1} + u_{ij}^{k-1} = & \lambda^2 a (u_{ij+1}^k + u_{ij-1}^k + u_{i+1j}^k + u_{i-1j}^k) + \\
 & + \lambda^2 b (u_{i+1j+1}^k + u_{i+1j-1}^k + u_{i-1j+1}^k + u_{i-1j-1}^k) + \lambda^2 c (u_{i+2j}^k + u_{i-2j}^k + u_{ij+2}^k + u_{ij-2}^k) + \\
 & + \lambda^2 d (u_{i+2j+1}^k + u_{i+2j-1}^k + u_{i-2j+1}^k + u_{i-2j-1}^k + u_{i+1j+2}^k + u_{i+1j-2}^k + u_{i-1j+2}^k + u_{i-1j-2}^k) + \\
 & + \lambda^2 e (u_{i+2j+2}^k + u_{i+2j-2}^k + u_{i-2j+2}^k + u_{i-2j-2}^k) + \lambda^2 f u_{ij}^k.
 \end{aligned} \tag{9}$$

For this scheme to approximate the wave equation to the fourth order, the parameters must satisfy the following relations:

$$\begin{aligned}
 a &= 14d + 32e + 4/3, & b &= -8d - 16e, \\
 c &= -2d - 2e - 1/12, & f &= 2/\lambda^2 - 24d - 60e - 5.
 \end{aligned}$$

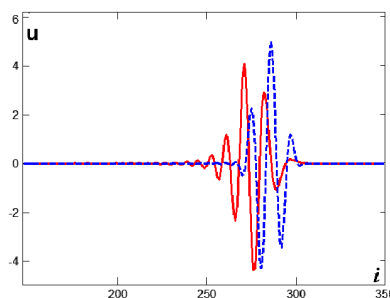
For the scheme to be direction-independent up to the sixth order of accuracy, an additional condition  $d/2 + 2e = -1/60$  must be satisfied. The parameter  $\lambda = -v\tau/h$  is determined from the Courant stability condition. The choice of the parameters  $d$  and  $e$  specifies various variants of the scheme. In this paper, for simplicity, we assume that  $d=0$ ; therefore,  $e=-1/120$ . The variant with  $d=0$  and  $e=0$  reduces the accuracy of the scheme but also reduces the computation time because the diagonal elements are excluded from the calculations.

Fig. 5 shows the results of the numerical simulations for the 2D case. The propagation of a short pulse in a homogeneous medium was computed using the 2<sup>nd</sup>-order

scheme (8) and the 4<sup>th</sup>-order scheme (9). The cross-sections of the pulse generated by the source according to formula (1) has the waveform shown in Fig. 4. Fig. 5 shows the cross-sections of the wave function  $u(\mathbf{r},t)$  perpendicular to the wave front at the same time step for the 2<sup>nd</sup>-order scheme (solid line) and the 4<sup>th</sup>-order scheme (dashed line). The X-axis shows the grid-point number. The computational domain size is  $200 \times 200$  mm, and the number of grid points is  $350 \times 350$ . The central wavelength of the pulse is 7 mm, so there are approximately 12 grid points per wavelength.



**Fig. 4.** Waveform of the sounding pulse.



**Fig. 5.** Cross-sections of the propagating waves for the 2<sup>nd</sup>-order (solid line) and 4<sup>th</sup>-order (dashed line) FDTD schemes.

The time moment in Fig. 5 is chosen so that the wave propagation distance reaches approximately 200 mm. It is evident that, for the 4<sup>th</sup>-order scheme, the distortion of the pulse is insignificant and that, for the 2<sup>nd</sup>-order scheme, the grid step turned out to be too large, which resulted in the distorted waveform and appearance of a "tail". If we use a grid that is two times finer in the 2<sup>nd</sup>-order scheme, we can obtain a waveform similar to that in Fig. 5 for the 4<sup>th</sup>-order scheme. Thus, the use of the 4<sup>th</sup>-order scheme makes it possible to reduce the grid size by a factor of 1.5–2 in each coordinate compared to the 2<sup>nd</sup>-order scheme for the problem of wave tomography, given parameters that are typical for medical imaging.

### 3.2 Transparency Conditions for the Boundary of the Computational Domain

When solving the "direct" (1)–(2) and "conjugate" (5)–(6) problems numerically, the boundary conditions must be applied at the boundary  $\partial\Omega$ . The boundary is assumed to be located far enough from the domain  $R$  such that during the time  $T$  the waves from the sources do not reach the boundary. In this case, the zero boundary conditions (2) are automatically satisfied. When carrying out the calculations, we can either choose a sufficiently large computational domain  $\Omega$  or assume that  $\Omega = R$ , which has a much smaller volume, and apply the non-reflecting ("transparent") boundary conditions.

In this paper, the numerical simulations are implemented with approximate non-reflecting boundary conditions. There are various options for the "transparency" con-

ditions [21-25]. The first option considered in this study is to create a border zone with a width of  $M$  grid points. Within this zone, an absorbing term  $a(\mathbf{r})u_i(\mathbf{r},t)$  is added to the left-hand side of the wave equation (1). The absorption coefficient quadratically increases for the points closer to the boundary  $\partial R$ .

The second option is to apply non-reflecting boundary conditions (NRBC) at the boundary of the computational domain. The exact NRBC formulation is non-local and is quite difficult to calculate. The first-order approximation of the NRBC has the form  $v \partial_n u|_{\partial R} = -\partial_t u|_{\partial R}$  and is exact for incident waves propagating perpendicular to the boundary. In this study, we use a second-order approximation, which has the form

$$\frac{\partial^2 u}{\partial x \partial t} - \frac{1}{v} \frac{\partial^2 u}{\partial t^2} + \frac{v}{2} \frac{\partial^2 u}{\partial y^2} = 0. \quad (10)$$

Fig. 6 shows the results of the 2D numerical simulations of a reflected pulse that has a width of 10 mm (25 grid points) and amplitude of 1. Fig. 6a shows the results of the first method (absorbing layer). The width  $M$  of the absorbing layer is 50 points in this case. Fig. 6b shows the results of the second method (10). The solid line shows the cross-section of the incident wave propagating perpendicular to the boundary, and the dashed line shows that of the wave propagating at a 45-degree angle.

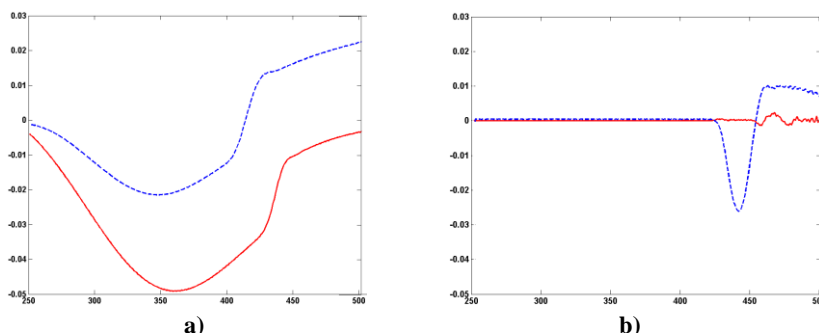


**Fig. 6.** The reflected waves for the 90-degree angle of incidence (solid line) and the 45-degree angle (dashed line): **a)** using an absorbing layer, **b)** using a 2<sup>nd</sup>-order approximate NRBC.

The X-axis shows the grid-point number, and the boundary is located at the right edge of the plots. The maximum amplitude of the reflections in Fig. 6a is 5%, and in Fig. 6b, it is 3%. In the second case, the reflections for the 90-degree angle of incidence are practically absent. In the first case, the reflected signal is almost 10 times wider than the original.

As follows from the numerical simulations, both methods allow us to approximate the boundary transparency condition with good accuracy, including steep angles of incidence. This made it possible to significantly reduce the size of the computational domain compared to the size at which the wave does not reach the boundary in time  $T$ . Even if a supercomputer is available, the reduction of the grid size is very im-

portant, especially in the 3D case, where the number of operations grows as  $n^4$  and the data volume grows as  $n^3$ .

### 3.3 The Iterative Process of Solving the Inverse Problem

The following iterative process was used to solve the inverse problem numerically. As the initial approximation, we use the value  $c^{(0)}=c_0=const$ , which corresponds to the speed of sound in pure water,  $v_0=1500 \text{ m}\cdot\text{s}^{-1}$ . At each iteration ( $m$ ), the following actions are performed:

1. The “direct” problem (1)–(2) is solved for the current approximation  $c^{(m)}$ . The propagation of the wave  $u^{(m)}(\mathbf{r},t)$  is computed using formula (8) or (9). The values of  $u(\mathbf{r},t)$  at each detector are computed.
2. The residual  $\Phi^{(m)}=\Phi(u^{(m)}(\mathbf{r}))$  is computed using formula (3).
3. The “conjugate” problem (5)–(6) is solved for  $w^{(m)}(\mathbf{r},t)$ . The gradient  $\Phi'_c(u^{(m)}(\mathbf{r}))$  is computed using formula (7) for all sources.
4. The current approximation is updated:  $c^{(m+1)}=c^{(m)}+\lambda^{(m)}\Phi'_c(u^{(m)}(\mathbf{r}))$ . The process returns to step 1.

The iteration process is stopped if the residual becomes smaller than some predetermined value, which corresponds to the a priori known precision of the measured data. The step of the gradient descent  $\lambda^{(m)}$  is chosen based on a priori considerations. Determining the step more precisely requires performing additional iterations and would increase the computation time by a factor of 2 or more. If the residual  $\Phi^{(m)}$  at the current iteration becomes larger than  $\Phi^{(m-1)}$ , the step  $\lambda^{(m)}$  is reduced by a factor of 1.5.

## 4 Numerical Simulations of Ultrasonic Tomography for the Second- and Fourth-Order FDTD Schemes

The numerical simulations for the 2D ultrasonic tomography problem were performed according to the scheme shown in Fig. 1. First, the direct problem of wave propagation through the simulated test object was solved using the 4<sup>th</sup>-order FDTD scheme (9). The wave field at the perimeter of the square (Fig. 1) was recorded and used as simulated measurement data to solve the inverse problem. The inverse problem was solved using both the 4<sup>th</sup>- and 2<sup>nd</sup>-order FDTD schemes. The approximate non-reflecting boundary condition (10) was applied.

The central wavelength of the pulse was 7 mm, the sound-speed range in the test object — 1430–1600  $\text{m}\cdot\text{s}^{-1}$ , the sound speed in the environment — 1500  $\text{m}\cdot\text{s}^{-1}$ , the size of the computational domain — 200×200 mm, and the size of the FDTD grid — 350×350 points. In the numerical simulations, we used eight sources that were located in the middle of each side of the square and in the corners of the square, as shown in Fig. 1. The detectors were located at the sides of the square with a pitch of 0.6 mm.

Fig. 7a shows an image of the simulated test object, Fig. 7b shows the image reconstructed using the 4<sup>th</sup>-order FDTD scheme, and Fig. 7c shows the image reconstructed using the 2<sup>nd</sup>-order FDTD scheme.

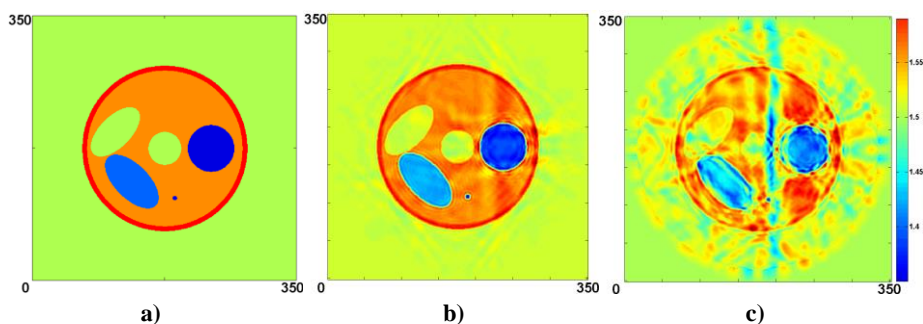


**Fig. 7.** a) Simulated test object, b) the image reconstructed using the 4<sup>th</sup>-order FDTD scheme, c) the image reconstructed using the 2<sup>nd</sup>-order FDTD scheme.

Comparing Fig. 7b and 7c, we can see that the numerical dispersion shown in Fig. 5 becomes significant for the 2<sup>nd</sup>-order FDTD scheme and significantly deteriorates the image quality, thus producing numerous artefacts. Using the 4<sup>th</sup>-order scheme allows the reconstruction of not only the shapes of irregularities but also the sound-speed function with high precision. Even small inclusions of size of 2–3 mm are reconstructed, and the precision of the sound speed reconstruction is  $10 \text{ m}\cdot\text{s}^{-1}$  or better.

The computing time for the 2D problem using eight computing cores of the “Lomonosov-1” supercomputer was approximately 2 hours for 400 iterations of the gradient method. Fig. 7c shows the result obtained after 150 iterations; then, the process stopped because the residual functional did not decrease any further.

The developed program for solving ultrasonic tomography problems is realized in the C++ language, designed for operation on high-performance cluster computer systems under the control of one of the Linux OS clones. For interprocessor exchange, the MPI interface was selected. Computations were carried out on the “Lomonosov-1” supercomputer of the Lomonosov Moscow State University Supercomputer Center on CPU Intel Xeon X5570 2.93GHz processors, 1.5 GB of memory per core, 8 x86 cores per node, Infiniband [26].

When carrying out computation in the problem under consideration on the CPU of the cluster system, it is natural to have a two-level parallelization based on the number of sources at the first level and then decomposition of the calculation area at the second level. This approach was implemented when performing computations with the 2<sup>nd</sup>-order FDTD scheme for 7-point stencil and showed high efficiency and scalability up to several tens of thousands of computing cores [14]. Moreover, scalability by sources is practically linear, since calculations for different sources are practically independent. When parallelizing the decomposition of the calculation area, it is necessary to perform data exchanges between neighboring regions, so the decomposition into too small areas is impractical. In the present work, in computations with the 4<sup>th</sup>-

order FDTD scheme for 27-point stencil, parallelization by sources was performed, which showed linear scalability. Parallelization by the technique of domain decomposition is supposed to be implemented in subsequent works.

As follows from the results of the work, using the 4<sup>th</sup>-order FDTD scheme allows us to reduce the size  $n$  of the computational grid by a factor of 1.5–2 compared to the 2<sup>nd</sup>-order scheme while maintaining the accuracy of the calculations. This fact is very important for inverse problems of wave tomography, especially in the 3D case, because the computation time increases as  $n^4$ . Although the increase of the stencil size causes approximately a two-fold increase of the computation time per grid point and a two-fold increase in inter-processor communications if the domain is divided among multiple processors, the number of grid points decreases by at least a factor of 3.

Moreover, for GPU processors, the memory requirement is a very important factor. For efficient GPU computing, all of the data used in the FDTD scheme must reside in the on-board memory of the GPU device. The volume of these data grows as  $n^3$  in the 3D case. The memory capacity limits the problem size to  $\sim 500^3$  points per computing node. This number of points is insufficient for precise calculations using a 2<sup>nd</sup>-order finite-difference scheme.

## 5 Conclusions

This paper is concerned with the optimization of numerical algorithms for solving the inverse problem of wave tomography using supercomputers. To reduce the computational grid dimensions, required memory capacity and computation time and to improve the accuracy of the calculations, the use of higher-order finite-difference schemes is proposed. It is shown that the fourth-order FDTD scheme allows us to decrease the grid size by a factor of 1.5–2 in each dimension compared to a second-order scheme while preserving the accuracy of the calculations. This approach significantly reduces both the computation time and the required memory capacity.

An important issue for numerical methods is the problem of boundary conditions for solving direct and inverse problems in a bounded domain. The article discusses two approximate methods that implement boundary "transparency". It is shown that both methods allow precise calculations and have significantly smaller computational complexities than exact non-reflecting boundary conditions.

The inverse problem is formulated as the incomplete-data tomography problem, where the sources and the detectors cannot be located on all sides of the examined object. To solve this important problem mathematically strictly, a method of calculating the gradient of the residual functional is proposed, which includes solving special "direct" and "conjugate" problems.

The proposed optimization scheme of the numerical algorithms is relevant due to the very large amount of computations required to solve the problems of wave tomography. The method is easy to implement on supercomputers.

**Acknowledgements.** This research was supported by Russian Science Foundation (project No. 17-11-01065). The study was carried out at the Lomonosov Moscow State University.

## References

1. Bazulin, A.E., Bazulin, E.G., Vopilkin, A.K., Kokolev, S.A., Romashkin, S.V., Tikhonov, D.S.: Application of 3D coherent processing in ultrasonic testing. *Russian journal of nondestructive testing* 50(2), 92–108 (2014).
2. Ruivo, G., Solimene, R., D'Alterio, A., Ammann, M.J., Pierri, R.: RF breast cancer detection employing a noncharacterized vivaldi antenna and a MUSIC-inspired algorithm. *Int J RF and Microwave Comp Aid Eng* 23, 598–609 (2012).
3. Tran-Duc, T., Linh-Trung, N., Do, M.N.: Modified Distorted Born Iterative Method for Ultrasound Tomography by Random Sampling. In: *International Symposium on Communications and Information Technologies (ISCIT)*, pp. 1065–1068. Gold Coast, QLD. (2012).
4. Goncharskii, A.V., Romanov, S.Y.: On a Three-Dimensional Diagnostics Problem in the Wave Approximation. *Computational Mathematics and Mathematical Physics* 40(9), 1308–1311 (2000).
5. Goncharskii, A.V., Ovchinnikov, S.L., Romanov, S.Y.: On the one problem of wave diagnostic. *Moscow University Computational Mathematics and Cybernetics* 34(1), 1–7 (2010).
6. Duric, N., Littrup, P., Li, C., Roy, O., Schmidt, S., Janer, R., Cheng, X., Goll, J., Rama, O., Bey-Knight, L., Greenway, W.: Breast ultrasound tomography: Bridging the gap to clinical practice. *Proc. SPIE. Medical Imaging: Ultrasonic Imaging, Tomography, and Therapy* 8320, 83200O (2012).
7. Gemmeke, H., Berger, L., Birk, M., Gobel, G., Menshikov, A., Tcherniakhovski, D., Zapf, M., Ruitter, N.V.: Hardware setup for the next generation of 3D ultrasound computer tomography. *IEEE Nucl. Sci. Symp. Conf. Rec.*, 2449–2454 (2010).
8. Wiskin, J., Borup, D., Andre, M., Johnson, S., Greenleaf, J., Parisky, Y., Klock, J.: Three-dimensional nonlinear inverse scattering: Quantitative transmission algorithms, refraction corrected reflection, scanner design, and clinical results. *J. Acoust. Soc. Am.* 133, 3229 (2013).
9. Natterer, F.: Possibilities and limitations of time domain wave equation imaging. *Contemporary Mathematics Providence: American Mathematical Society* 559, 151–162 (2011).
10. Natterer, F.: *Sonic Imaging*. In: *Handbook of Mathematical Methods in Imaging*, pp. 1253–1278. Springer-Verlag, New York (2015).
11. Beilina, L., Klibanov, M.V., Kokurin, M.Y.: Adaptivity with relaxation for ill-posed problems and global convergence for a coefficient inverse problem. *J. Math. Sci.* 167, 279–325 (2010).
12. Beilina, L., Klibanov, M.V.: *Approximate global convergence and adaptivity for coefficient inverse problems*. Springer, New York (2012).
13. Goncharskii, A.V., Romanov, S.Y.: Two approaches to the solution of coefficient inverse problems for wave equations. *Comput. Math. Math. Phys.* 52, 245–51 (2012).
14. Goncharsky, A.V., Romanov, S.Y.: Supercomputer technologies in inverse problems of ultrasound tomography. *Inverse Probl.* 29(7), 075004 (2013).

15. Goncharsky, A.V., Romanov, S.Y.: Inverse problems of ultrasound tomography in models with attenuation. *Phys. Med. Biol.* 59(8), 1979–2004 (2014).
16. Goncharsky, A.V., Romanov, S.Y., Seryozhnikov, S.Y.: Inverse problems of 3D ultrasonic tomography with complete and incomplete range data. *Wave Motion* 51(3), 389–404 (2014).
17. Goncharsky, A.V., Romanov, S.Y., Seryozhnikov, S.Y.: A computer simulation study of soft tissue characterization using low-frequency ultrasonic tomography. *Ultrasonics* 67, 136–150 (2016).
18. Goncharskii, A.V., Romanov, S.Y., Seryozhnikov, S.Y.: Low-Frequency Three-Dimensional Ultrasonic Tomography. *Doklady Physics* 61(5) 211–214 (2016).
19. Goncharsky, A.V., Romanov, S.Y.: Iterative methods for solving coefficient inverse problems of wave tomography in models with attenuation. *Inverse Problems* 33(2), 025003 (2017).
20. Bilbao, S.: *Numerical Sound Synthesis: Finite Difference Schemes and Simulation in Musical Acoustics*. A John Wiley and Sons, Ltd, Chichester (2009).
21. Manolis, G.D., Beskos, D.E.: *Boundary Element Methods in Elastodynamics*. Unwin Hyman, London (1988).
22. Givoli, D., Keller, J.B.: Non-reflecting boundary conditions for elastic waves. *Wave Motion* 12(3), 261–279 (1990).
23. Clayton, R., Engquist, B.: Absorbing boundary conditions for acoustic and elastic wave equations. *Bulletin of the Seismological Society of America* 67(6), 1529–1540 (1977).
24. Engquist, B., Majda, A.: Absorbing boundary conditions for the numerical simulation of waves. *Math. Comput.* 31, 629 (1977).
25. Alpert, B., Greengard, L., Hagstrom, T.: Boundary Conditions for the Time-Dependent Wave Equation. *Journal of Computational Physics* 180, 270–296 (2002).
26. Sadovnichy, V., Tikhonravov, A., Voevodin, V., Opanasenko, V.: "Lomonosov": Supercomputing at Moscow State University. In: *Contemporary High Performance Computing: From Petascale toward Exascale*, Edited by Jeffrey S. Vetter, pp. 283–307. Chapman and Hall/CRC, Boca Raton, United States (2013).